

Hydrogen bonding network in a chiral alcohol: (1R,2S,5R)-(–)-menthol. Conformational preference studied by IR–Raman–VCD spectroscopies and quantum chemical calculations

Juan Ramón Avilés Moreno · Francisco Partal Ureña ·
Juan Jesús López González

Received: 20 April 2012 / Accepted: 24 August 2012 / Published online: 9 September 2012
© Springer Science+Business Media, LLC 2012

Abstract A study of the molecular structure of (1R,2S,5R)-(–)-menthol and the hydrogen bond networks formed by this species in solution is carried out. Molecular structures of monomers and H-bonded dimers and trimers of the title compound are optimized using quantum chemical calculations in the isolated molecule approach. In addition, IR, Raman and VCD techniques are used to study CCl₄ solutions and thin films of the target compound. Their corresponding vibrational spectra are then analysed, both theoretically (HF and DFT) and experimentally, to characterize the different monomers (rotamers) and H-bonded oligomer species in menthol solutions as a function of the concentration.

Keywords Chiral alcohol molecular conformation · (1R,2S,5R)-(–)-Menthol · H-Bonding network · VCD · IR · Raman

Introduction

The substance known as (1R,2S,5R)-(–)-menthol (Fig. 1) is a monoterpene [1, 2] found in mint oils. (–)-Menthol plays an important role in many biological processes and asymmetric reactions and shows analgesic and vasodilating properties [3–5].

The structure of menthol has been investigated by X-ray diffraction [6], NMR [7], and IR spectroscopy [8, 9]. Recent work by Albrecht et al. [9] is focused on the aggregates of menthol and neomenthol in the gas phase.

Using VCD spectroscopy, the molecular structure of (1S,2R,5S)-(+)-menthol has been investigated by several authors [10–16]. Among them, Mc Cann et al. [15, 16] presented a study focused on the monomer structure in CCl₄ solution (0.4 M), corresponding to equatorial monomers; these authors did not analyse the O–H stretching region, even though the existence of an H-bonding network can be expected.

Other previous works deal with the structure–spectra relationship in menthol or its derivatives, using VCD spectroscopy [12], ROA spectroscopy [17], matrix isolation Fourier transform infrared (MI-FTIR) spectroscopy [18] or optical rotation [19].

Our aim was to determine the structure and the conformational landscape of its monomers and aggregates in solution. Hence, this work studies the H-bonding network in (1R,2S,5R)-(–)-menthol [20–26] by means of IR, Raman and VCD spectroscopies, combined with quantum chemical calculations. As a first step, a theoretical investigation on the conformational landscape of menthol monomers, their Boltzmann populations and their IR, Raman and VCD spectra is carried out. Then, IR, Raman and VCD spectra were recorded in the solid phase (thin films) and in CCl₄ solutions at different concentrations.

Electronic supplementary material The online version of this article (doi:10.1007/s11224-012-0118-8) contains supplementary material, which is available to authorized users.

J. R. Avilés Moreno (✉) · F. Partal Ureña ·

J. J. López González

Grupo de Química Física Teórica y Experimental,
Departamento de Química Física y Analítica, Facultad de
Ciencias Experimentales, Universidad de Jaén, Edificio B3.,
Campus Las Lagunillas, 23071 Jaén, Spain
e-mail: jraviles@ujaen.es

F. Partal Ureña

e-mail: fpartal@ujaen.es

J. J. López González

e-mail: jjlopezl@ujaen.es

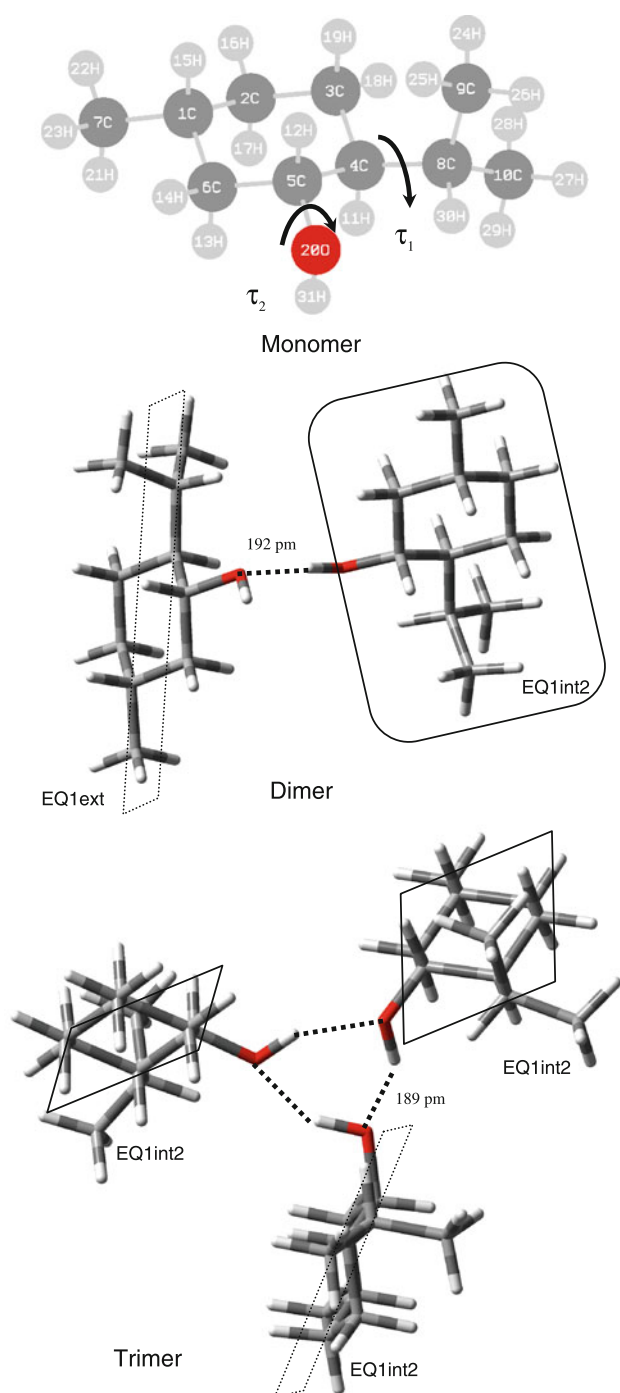


Fig. 1 Molecular structure of the monomer, dimer and trimer and atom numbering adopted in this study for (1R,2S,5R)-(–)-menthol. Dotted lines show the H-bond (Color figure online)

Experimental details

Commercial (1R,2S,5R)-(–)-menthol samples (99 %) were purchased from Sigma-Aldrich. IR, Raman and VCD spectra were recorded without further purification in different conditions:

- CCl_4 solutions were prepared from 0.01 to 1.80 M.
- The solid phase, using thin films, was obtained from a very low concentration solution of the sample on BaF_2 windows [27]. The solvent was evaporated under anhydrous conditions.

To record the IR spectra, we used an FT-IR Bruker Vector 22 spectrometer, equipped with a Globar source, CsI optics and a DGTS detector. The IR spectra were recorded in the $400\text{--}4,000\text{ cm}^{-1}$ range, with a resolution of 1 cm^{-1} and 200 scans.

Raman spectra were recorded using a Bruker RF100/S FT-Raman spectrometer equipped with an Nd:YAG laser (excitation line at 1,064 nm) and a Ge detector cooled at liquid nitrogen temperature. The spectra were measured using a standard liquid cell with a resolution of 1 cm^{-1} and 200 scans.

VCD spectra were recorded using a JASCO FVS-4000 FTIR spectrometer equipped with InSb ($4,000\text{--}1,900\text{ cm}^{-1}$) and MCTV ($2,000\text{--}900\text{ cm}^{-1}$) detectors. All spectra were recorded using a standard cell equipped with BaF_2 windows, with a resolution from 2 to 8 cm^{-1} , path lengths between 6 and $100\text{ }\mu\text{m}$, and from 2,000 to 16,000 scans. For the baseline correction, we subtracted the solvent spectrum from the solution spectra [28]. We present another usual baseline correction taking into account (–)- and (+)-menthol for comparison (Fig. 1S). From the raw spectra, the half-sum of the VCD enantiomer spectra is subtracted; this half-sum is mathematically defined as $[\Delta A(R) + \Delta A(S)]/2$. The corrected VCD spectra are thus similar to those obtained using the previous correction and to the spectra documented in previous works [10, 15].

In the case of thin films, we subtracted the empty cell spectrum from the film spectra [27].

Computational details and methods

All the theoretical calculations were carried out using the Gaussian03 software package [29].

In a first step, a fixed scan of the potential energy surface (PES) was performed for the monomers of (1R,2S,5R)-(–)-menthol at the B3LYP/6-31G** level of theory. Rotations along the τ_1 (C9–C8–C4–C3, rotation of the isopropyl group with respect to the ring) and τ_2 (H31–O20–C5–C4, rotation of the hydroxyl group with respect to the ring) dihedral angles were studied, maintaining the rest of the structural parameters. As an example, Fig. 2S shows the PES obtained for the equatorial and axial conformers. Both scans gave three different positions of the O–H group with respect to the ring.

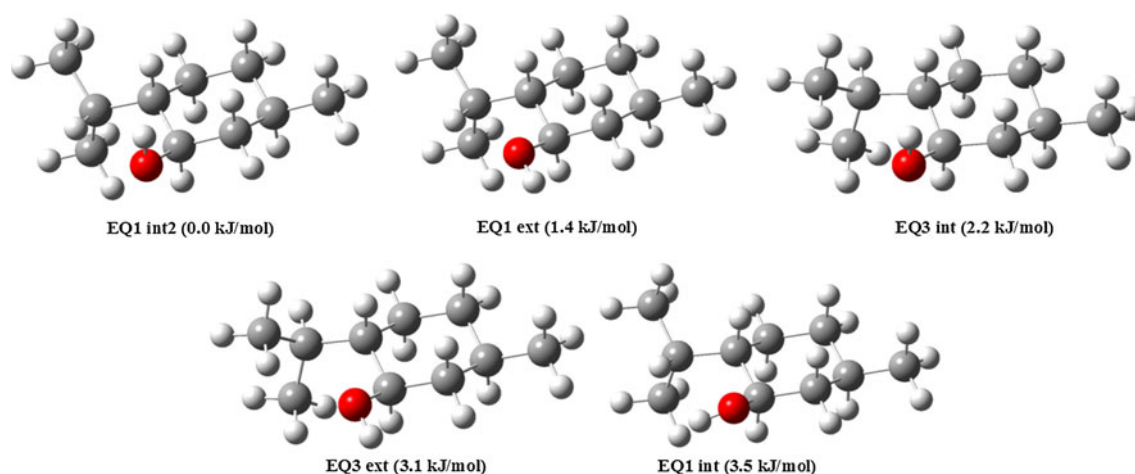


Fig. 2 Structure of the five most stable conformers of (1R,2S,5R)-(-)-menthol at the B3LYP/cc-pVDZ level of theory. Relative energies with ZPE corrections are shown for each (Color figure online)

Afterwards, a re-optimization of the structure and calculation of the relative energies (with ZPE correction) and Boltzmann populations of all the conformers found were done at the B3LYP/cc-pVDZ and B3LYP/6-31G* levels. Harmonic IR, Raman and VCD spectra were predicted at the same level of theory. Stephens' theory [30] was used to obtain VCD spectra, as implemented in Gaussian03 [29].

Solvent effects (CCl₄) were taken into account using the IEF-PCM methodology [31] implemented in Gaussian03.

Pulay's Scaled Quantum Mechanical Force Field (SQMFF) methodology [32] was used for the vibrational analysis, along with MOLVIB software [33, 34]. Calculated force fields in Cartesian coordinates at the B3LYP/cc-pVDZ level were first written in terms of Pulay's natural internal coordinates. Afterwards, theoretical values of the wavenumbers of the most stable rotamers were fitted to the experimental ones. The results thereby predicted VCD spectra at the same level of theory, with the aid of MakeVCD software by JASCO Inc. [35].

To reproduce the H-bonding spectra features of (1R,2S,5R)-(-)-menthol, the structures of small oligomers (dimers and trimers) were optimized at the HF/6-31+G* and B3LYP/6-31+G* levels of theory, and similarly as for the monomer, the relative energies (with ZPE correction) and the harmonic IR–Raman–VCD spectra of the dimer and trimer structures were calculated at the B3LYP/6-31+G* level. The starting point for optimization of the oligomers was the structure of the most stable rotamer of the monomer, i.e. EQ1int2. Due to the dimensions of the problem (dimers and trimers have 62 and 93 atoms, respectively), the B3LYP/6-31+G* level is a reasonable choice in terms of computational cost [23].

For comparison purposes, selected monomer structures were optimized so that their spectra could be obtained at the same level as the dimer and trimer, i.e. B3LYP/6-31+G*.

Results and discussion

Conformational analysis

At the B3LYP/cc-pVDZ level of the theory, the monomer of menthol presents 18 stable conformers depending on the position of the isopropyl group with respect to the six-membered ring (equatorial or axial position) and the orientation of the O–H group (towards the ring or towards the opposite direction; see Fig. 1). In view of the ZPE corrected energy at the same level of theory, it is clear that the equatorial conformers are more stable than the axial ones (see Fig. 2).

Table 1 shows the calculated molecular populations of the nine most stable rotamers (all of them equatorial). Meanwhile, Table 1S shows the molecular parameters (in terms of Z-matrix) of the five most stable rotamers. Here, the torsion angle of the isopropyl group ($\tau_1 = \text{C9–C8–C4–C3}$) and the hydroxyl group ($\tau_2 = \text{H31–O20–C5–C4}$) have respective values of 54.9° and 294.8° (EQ1int2), 57.3° and 180.1° (EQ1ext), 206.2° and 295.7° (EQ3int), 209.2° and 180.4° (EQ3ext), 58.9° and 70.3° (EQ1int). The results of the IEF-PCM (CCl₄ effect) methodology at the B3LYP/cc-pVDZ reveals that the five most stable conformers and their relative energies (with ZPE correction) are comparable to those obtained under the isolated molecule approach.

As shown in the next section, IR and VCD spectra features change depending on the experimental conditions, due to changes in the H-bonding network in solution. We optimized the structure of small oligomers (dimers and trimers) of menthol, along the lines of previous work with other alcohols [9, 23, 25], at the HF and B3LYP levels of theory using the 6-31+G* basis set (see Fig. 1; Table 2S).

The length of the hydrogen bond is 192 pm for the dimer (one H-bond), and 189 pm for the trimer (three

Table 1 Calculated molecular populations and relative energies (with ZPE correction) and structural parameters for the nine most stable equilibrium structures optimized at the B3LYP/cc-pVDZ (isolated and PCM with CCl₄) and B3LYP/6-31+G* levels of theory for (1R,2S,5R)-(-)-menthol

Conformer	B3LYP/cc-pVDZ					B3LYP/6-31+G*	B3LYP/cc-pVDZ PCM CCl ₄
	ΔE_c (kJ/mol)	ΔE_0 (kJ/mol)	% Population ^a	τ_1 (°)	τ_2 (°)	ΔE_0 (kJ/mol)	ΔE_0 (kJ/mol)
EQ1int2	0.0	0.0	37.7	55	-65	0.9	0.4
EQ1ext	1.8	1.4	21.6	57	-180	0.0	0.0
EQ3int	1.9	2.2	15.3	-154	-64	5.0	5.0
EQ3ext	2.9	3.1	10.8	-151	-180	4.3	4.5
EQ1int	4.1	3.5	9.1	59	70	2.4	1.5
EQ2int	6.9	7.2	2.1	-41	-65	10.9	10.8
EQ3int2	7.6	7.4	1.9	-150	76	8.5	8.0
EQ2ext	8.8	8.8	1.1	-31	180	9.6	10.0
EQ2int2	10.8	11.2	0.4	-26	73	12.9	12.4

^a Boltzmann population from ΔE_0 taking $T = 298.16$ K

H-bonds), at the B3LYP/6-31+G* level of theory, indicating they are mid-strength H-bonds [24]. Dissociation energies for the dimer and trimer are estimated to be around 17 and 50 kJ/mol, respectively. It is important to stress that the dimer presents one intermolecular H-bond and the trimer presents three intermolecular H-bonds, i.e. the dissociation energy per H-bond is approximately 17 kJ/mol. In the dimer, the two rings present a twisted orientation with an angle around 90° between them. The optimized dimer structure is in good agreement with the one recently described by Albrecht et al. [9]. In the trimer, the three rings present a twisted orientation with respect to the plane formed by the three oxygen atoms involved in the corresponding H-bonds, with a torsion angle around 90°.

Spectra features

As can be seen in Fig. 3 (1R,2S,5R)-(-)-menthol displays rather complex IR and Raman spectra. In addition, relevant changes are seen in the IR spectra within the 3,700–3,000 cm⁻¹ region, depending on the concentration of menthol in CCl₄ (thin films and solutions with concentrations from 0.6 to 0.01 M). These alterations are due to the presence of different species involved in H-bonding networks [28, 36].

Thus, a previous assignment of the IR and Raman spectra of the 0.03 M solution (see Tables 2, 3S) is done in terms of the five most stable equatorial rotamers (EQ1int2, EQ1ext, EQ3int, EQ3ext and EQ1int, see Fig. 2) of menthol. For the monomer, the theoretical IR–Raman–VCD spectra were constructed taking into account the Boltzmann weights of the five most stable rotamers.

Monomers of menthol have 87 vibrational normal modes belonging to the unique irreducible representation (A) of the symmetry point group, C₁. To carry out the

vibrational analysis, we transferred a set of scaling factors coming from the analysis of similar terpenes obtained by our group [37–42]. To improve the root means square (RMS) error, two new scaling factors were refined: they were those associated to the O–H–C bending and O–H stretching force constants by fitting the theoretical values of the wavenumbers to those of the bands assigned (in the recorded IR and Raman spectra) to the normal modes of these vibrations for the five most stable rotamers of the menthol (Table 3), giving an average RMS of 5.6 cm⁻¹ for the set of them. The predicted scaled average spectrum for the five most stable rotamers reproduces the experimental one, with the exception of the O–H region, where features associated with H-bonded oligomers are found. Table 4S shows the output of the MOLVIB program for the five rotamers, while Table 5S displays the Potential Energy Distribution Matrix (PEDM) of each normal mode.

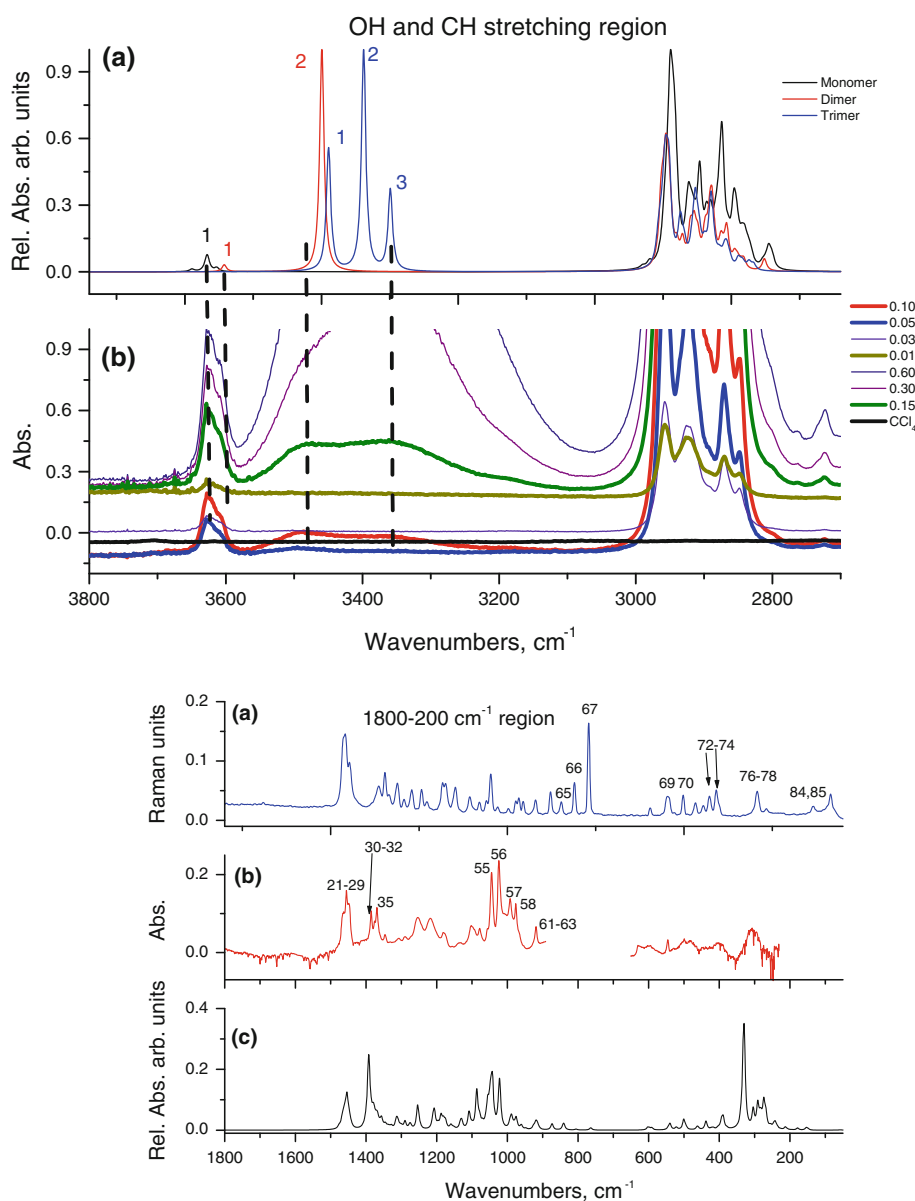
For the sake of clarity, in this study the spectral range is divided into two zones.

O–H and C–H stretching region

Figure 3 clearly shows that the O–H stretching related to the monomer appears in the spectra of the more diluted CCl₄ solutions (0.01 and 0.03 M). Normal mode 1 (O–H stretching) has been assigned for the five most stable rotamers to the three first bands observed when working in diluted solutions of menthol in CCl₄ (Fig. 3) at 3,644 cm⁻¹ (sc. 3,646 cm⁻¹ and unsc. 3,791 cm⁻¹ for EQ1int), 3,623 cm⁻¹ (sc. 3,628–3,622 cm⁻¹ and unsc. 3,772–3,766 cm⁻¹ for EQ1ext and EQ3ext, respectively) and 3,609 cm⁻¹ (sc. 3,607–3,602 cm⁻¹ and unsc. 3,751–3,745 cm⁻¹ for EQ3int and EQ1int2, respectively).

In contrast, broad bands due to H-bonded oligomers appear at higher concentrations (0.30 and 0.60 M) and thin

Fig. 3 Experimental IR and Raman spectra compared with predicted scaled spectrum for (1R,2S,5R)-(-)-menthol in the 3,800–100 cm^{-1} . **Top a** sum of the predicted scaled IR spectra of the five most stable conformers (SQMFF methodology, in black); predicted IR spectra of the dimer (in red) and the trimer (in blue); **b** experimental IR spectrum (resolution of 1 cm^{-1} and 200 scans) of different solutions in CCl_4 (in molar concentration). Dotted lines show the positions of the O–H bands found. **Bottom a** experimental Raman spectrum (in blue, solid phase, resolution of 1 cm^{-1} and 200 scans); **b** experimental IR spectrum (in red, CCl_4 solution 0.03 M, resolution of 1 cm^{-1} and 200 scans); and **c** sum of the predicted scaled IR spectra of the five most stable conformers taking into account their contributions according to Boltzmann's populations at 298.16 K. (pitch = 1 cm^{-1} , FWHM = 8 cm^{-1}). Dotted line shows the position of the free O–H stretching (Color figure online)



films. For the dimer (see the structure in Fig. 1 and the assignment in Table 2), the B3LYP/6-31+G* calculation (without any scaling of the wavenumbers) predicts two bands. The first is a weak band around 3,744 cm^{-1} (unsc. and sc. 3,609 cm^{-1}), assigned to the O–H stretching of the acceptor hydroxyl group. The second band is stronger and is predicted around 3,601 cm^{-1} (unsc. and sc. 3,471 cm^{-1} , normal mode 2, around 143 cm^{-1} lower than the acceptor O–H stretching). This band is assigned to the O–H stretching of the donor hydroxyl group. In the recorded spectra (0.60 and 0.30 M solutions), we detect two bands at 3,609 cm^{-1} (overlapped with O–H bands related to the monomers EQ3int and EQ1int2) and 3,491 cm^{-1} , which appears 118 cm^{-1} below and in good agreement with the calculations.

For the trimer (Fig. 1; Table 2), the B3LYP/6-31+G* calculation predicts three bands related to the O–H stretchings around 3,591 cm^{-1} (unsc. and sc. 3,462 cm^{-1} , normal mode 1), 3,540 cm^{-1} (unsc. and sc. 3,413 cm^{-1} , normal mode 2) and 3,501 cm^{-1} (unsc. and sc. 3,384 cm^{-1} , normal mode 3). The predicted differences are around 50 and 40 cm^{-1} , respectively, between normal modes 1 and 2, and 2 and 3. Experimentally, we detected a broad band centred at 3,314 cm^{-1} , which can be assigned to the normal modes 2 and 3 of the trimer, and another broad band at 3,491 cm^{-1} , assigned to normal mode 1 of the trimer and normal mode 2 of the dimer.

Figure 4 shows two experimental VCD spectra in the O–H stretching (3,800–3,100 cm^{-1}) and C–H stretching (3,200–2,600 cm^{-1}) regions in CCl_4 solutions. In addition,

Table 2 Theoretical scaled and experimental IR and Raman vibrational wavenumbers (cm^{-1}) of (1R,2S,5R)-(–)-menthol for the five most stable rotamers of the monomer, dimer and trimer

IR liquid CCl_4 solution	Relative intensity	Raman solid	Relative intensity	Monomer			Dimer	Trimer	Assignment ^a
				Conformer	B3LYP/cc-pVDZ	SQMFF scaled			
3,644 ^a	vw			EQ1int	3,791	3,644			O–H stretching monomers
3,623 ^a	w			EQ1ext	3,773	3,623			
				EQ3ext	3,766	3,623			
3,609	w			EQ3int	3,751	3,609	3,744		O–H stretching monomers + free O–H stretching dimer
				EQ1int2	3,745	3,609			
3,491	w						3,601		Linked O–H stretching dimer
Broad band								3,591	Asym. O–H stretching trimer
3,314	w							3,540	Asym. O–H stretching trimer
Broad band								3,501	Asym. O–H stretching trimer
2,957	s	2,960	s		3,102–3,027	2,978–2,907			C–H stretching of the methyl and methylene groups for the five rotamers
–		2,951	sh						
2,922	s	2,930	s						
–		2,910	s						
–		2,859	s		2,976–2,950	2,857–2,832			
2,848	s	2,846	s						
–		2,829	vw						
1,464	m	1,461	s		1,483–1,454	1,468–1,440			Isopropyl def. + CH_3 sym. and asym. def. CH_3 scissoring for the five rotamers
1,456	m	–							
1,448	m	1,447	s						
1,402	m	–			1,427	1,414			C10H_3 sym. def. of EQ1ext, EQ3ext and EQ1int
1,386	m	–			1,406	1,392			C10H_3 sym. def. of EQ1int2 and EQ3int
1,308	m	1,311	m		1,335–1,289	1,322–1,275			CH_3 wagging + twisting + rocking for the five rotamers
1,290	m	1,292	m						
1,271	m	1,271	m						
1,045	m	1,047	m		1,061	1,044			C5-O20 stretching + ring deformation for the five rotamers
1,024	m	1,027	w		1,042	1,025			

See Tables 2S, 3S, 4S and 5S in the supporting information for additional data

vs very strong, s strong, m medium, w weak, vw very weak, sh shoulder

^a See text and Tables 3S, 4S and 5S for more explanation about the vibrational assignment

^b Data coming from the IR spectrum in CCl_4 solution (see Fig. 3)

Figs. 3S and 4S compare the predicted IR–VCD spectra in the whole range for the monomer—taking into account the five most stable rotamers (panel a), the dimer (panel b) and the trimer (panel c). The VCD spectrum in panel c1 (0.30 M solution) shows a (–, +) VCD pattern around $3,630 \text{ cm}^{-1}$, assigned to normal mode 1 of the five most stable rotamers of the monomer.

Concerning the O–H stretching region, in panel b1 (1.80 M solution) we likewise see the aforementioned pattern around $3,630 \text{ cm}^{-1}$ (it becomes weaker). New VCD bands appear around $3,400\text{--}3,300 \text{ cm}^{-1}$: a positive band at

$3,436 \text{ cm}^{-1}$, which could be assigned to normal mode 2 of the dimer; a negative band at $3,374 \text{ cm}^{-1}$ and another positive band at $3,324 \text{ cm}^{-1}$, which in turn could be assigned to normal modes 1, 2 and 3 of the trimer (see Table 2). The remaining VCD bands in this region could be assigned as overtones and/or bands due to other oligomers.

The next four bands appearing at higher wavenumbers in the IR and Raman spectra, $2,957 \text{ cm}^{-1}$ (IR, $2,960 \text{ cm}^{-1}$ Raman), $2,951 \text{ cm}^{-1}$ (Raman), $2,922 \text{ cm}^{-1}$ (IR, $2,930 \text{ cm}^{-1}$ Raman) and $2,910 \text{ cm}^{-1}$ (Raman) (Tables 2, 3S), are assigned to the C–H stretchings (symmetric and asymmetric)

Table 3 Set of scaling factors obtained for (1R,2S,5R)-(–)-menthol at B3LYP/cc-pVDZ level of theory for the five most stable rotamers and the mean value of the RMS

Scaling factor	Menthol		Mean value four terp. ^b	Mean value five terp. ^c
	Transferred ^a	Partially fitted		
C=C stretching	–	–	0.904	0.904
C–C stretching	0.967	–	0.967	0.967
C–H stretching	0.923	–	0.923	0.923
X–Y–Z bending	0.996	–	0.996	0.996
Torsions of single bonded systems	0.994	–	0.994	0.994
X–Y–H bending	0.979	–	0.979	0.979
Out-of-plane modes	0.966	–	0.966	0.966
H–X–H bending	0.980	–	0.980	0.980
Torsions of conjugated systems	0.924	–	0.924	0.924
O–H–C bending	0.88	1.000	–	0.940
C–O stretching	0.945	–	0.945	0.945
O–H stretching	0.935	0.925	–	0.930
Mean RMS (cm ⁻¹)	6.0	5.6	–	–

^a Mean value transferred for the five most stable rotamers of menthol analysed

^b Mean value obtained from the analysis of four terpenes: limonene, limonene oxide, carvone and perillaldehyde

^c Mean value obtained from the analysis of four terpenes + menthol

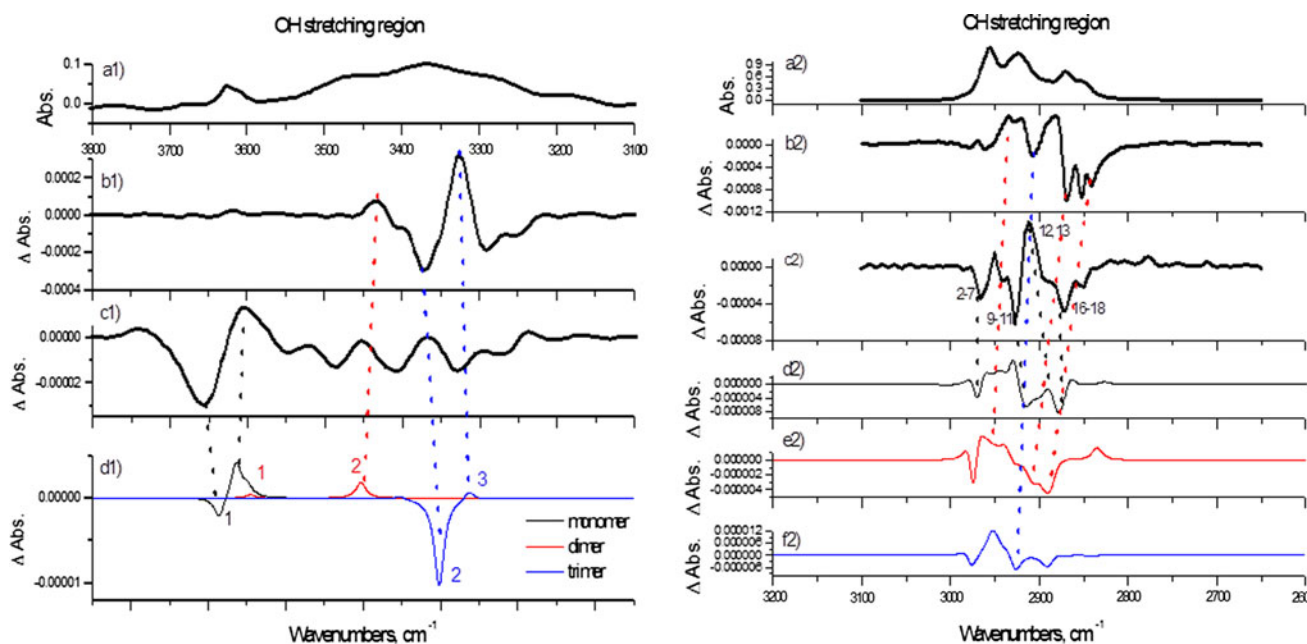


Fig. 4 Experimental and theoretical IR–VCD spectra of (1R,2S,5R)-(–)-menthol in the O–H stretching (3,800–3,100 cm⁻¹) and C–H stretching (3,200–2,600 cm⁻¹) regions: recorded IR (**a1**) and VCD (**b1**) spectra (2,000 scans, 16 cm⁻¹ of resolution, spacer of 0.5 mm, 1.80 M in CCl₄); **c1** recorded VCD spectrum (2,000 scans, 16 cm⁻¹ of resolution, spacer of 0.5 mm, 0.30 M in CCl₄); **d1** averaged sum of the predicted scaled spectra of the five most stable rotamers of the monomer (SQMFF methodology, in black), predicted spectra of the dimer (in red)

and trimer (in blue); recorded IR (**a2**) and VCD (**c2**) spectra (2,000 scans, 8 cm⁻¹ of resolution, spacer of 0.5 mm, 0.15 M in CCl₄ and narrow band CH filter); **b2** Recorded VCD spectrum (thin film, 2,000 scans, 4 cm⁻¹ of resolution, narrow band CH filter); **d2** averaged sum of the predicted scaled spectra of the five most stable rotamers of the monomer (SQMFF methodology in black); predicted scaled spectra of the dimer (**e2**, in red) and trimer (**f2**, in blue) (unique wavenumber scaling factor of 0.964 [43]). Parameters: pitch = 1 cm⁻¹, FWHM = 8 cm⁻¹ (Color figure online)

of the methyl groups (containing C9, C7 and C10) and of the methylene groups (containing C3, C6 and C2), and normal modes 2–12 of the five most stable monomers

(Tables 2, 3S, 5S). The corresponding scaled and unscaled values are: 2,978–2,907 cm⁻¹ and 3,102–3,027 cm⁻¹, respectively.

The next three bands at $2,859\text{ cm}^{-1}$ (Raman), $2,848\text{ cm}^{-1}$ (IR, $2,846\text{ cm}^{-1}$ Raman) and $2,829\text{ cm}^{-1}$ (Raman) are assigned to the C–H stretchings of methine groups containing C1, C5 and C4 (normal modes 19 and 20) of the five most stable monomers. The corresponding scaled and unscaled values are: $2,857\text{--}2,832\text{ cm}^{-1}$ and $2,976\text{--}2,950\text{ cm}^{-1}$. In view of the theoretical calculations, and dimer and trimer C–H stretching the wavenumbers resemble those for the same movement of the different rotamers of the monomer.

For this region, VCD signals in the spectrum corresponding to the solution 0.15 M (Fig. 4, c2) are assigned to the five most stable rotamers of the monomer (bands marked with dotted lines). As examples, the negative band at $2,965\text{ cm}^{-1}$ is assigned to normal modes 2–7, the negative band at $2,927\text{ cm}^{-1}$ is assigned to normal modes 9–11, the positive band at $2,911\text{ cm}^{-1}$ is assigned to normal modes 12 and 13 and the negative band at $2,873\text{ cm}^{-1}$ is assigned to normal modes 16–18.

Figure 4b2 shows the VCD spectrum of (–)-menthol in thin film conditions, which present some different features with respect to the solution spectrum. For instance, the positive VCD bands at $2,934$ and $2,920\text{ cm}^{-1}$, as well as the negative band at $2,869\text{ cm}^{-1}$, could be assigned to the presence of the dimer and trimer (see Fig. 4, red and blue dotted lines). Accordingly, the VCD technique provides greater insight than IR and Raman with regard to the presence of different menthol species.

Intermediate and low-frequency region (below $2,000\text{ cm}^{-1}$)

In this region, the normal modes have a complex description from the PEDM: symmetric and asymmetric angle deformations and (heavy atom) bond stretchings, scissoring, wagging, rocking, etc. From the theoretical calculations, as in the previous region, dimers and trimers present wavenumbers and descriptions close to those derived through theoretical calculations for the same vibrations of the different rotamers of the monomer.

The first three bands (Fig. 3) with the highest wavenumbers in this zone, i.e. those at $1,464\text{ cm}^{-1}$ (IR, and $1,461\text{ cm}^{-1}$ Raman), at $1,456\text{ cm}^{-1}$ (IR) and $1,448\text{ cm}^{-1}$ (IR, $1,447\text{ cm}^{-1}$ Raman), are assigned to the normal modes 21–26 for the five most stable rotamers; they correspond to isopropyl deformation, symmetric and asymmetric deformation of the methyl groups, and scissoring of these groups. The corresponding scaled and unscaled values are: $1,468\text{--}1,440\text{ cm}^{-1}$ and $1,483\text{--}1,454\text{ cm}^{-1}$, respectively.

Other bands in this region are the one at $1,402\text{ cm}^{-1}$ (IR, $1,427\text{ cm}^{-1}$ unsc. and sc. $1,414\text{ cm}^{-1}$), assigned to normal mode 30 (symmetric deformation of methyl containing C10) of rotamers EQ1ext, EQ3ext and EQ1int, and the band at $1,386\text{ cm}^{-1}$ (IR, $1,406\text{ cm}^{-1}$ unsc. and sc.

$1,392\text{ cm}^{-1}$), assigned to the same mode of rotamers EQ1int2 and EQ3int.

Further examples are bands at $1,308\text{ cm}^{-1}$ (IR, $1,311\text{ cm}^{-1}$ Raman), $1,290\text{ cm}^{-1}$ (IR, $1,292\text{ cm}^{-1}$ Raman) and $1,271\text{ cm}^{-1}$ (IR and Raman), all assigned to normal modes 40–43 (wagging, twisting and rocking of the methyl groups, see Tables 3S, 4S, 5S). The corresponding scaled and unscaled values are, respectively, $1,322\text{--}1,275\text{ cm}^{-1}$ and $1,335\text{--}1,289\text{ cm}^{-1}$. The bands at $1,045\text{ cm}^{-1}$ (IR, $1,047\text{ cm}^{-1}$ Raman) and $1,024\text{ cm}^{-1}$ (IR, $1,027\text{ cm}^{-1}$ Raman) are in turn assigned to normal modes 55 and 56 (C5–O20 stretching mixed with six-ring deformation) for the five most stable rotamers. In this case, the scaled values are $1,044$ and $1,025\text{ cm}^{-1}$ and the corresponding unscaled ones are $1,061$ and $1,042\text{ cm}^{-1}$.

Figure 5 gives three experimental VCD spectra (b, 0.40 M; c, 1.20 M; d, thin film) in the intermediate region ($2,000\text{--}900\text{ cm}^{-1}$) along with the predicted VCD spectra of the monomer (e, taking into account the five most stable rotamers), the dimer (f) and the trimer (g). For the dimer and trimer, a unique wavenumber scaling factor of 0.964 [43] was used.

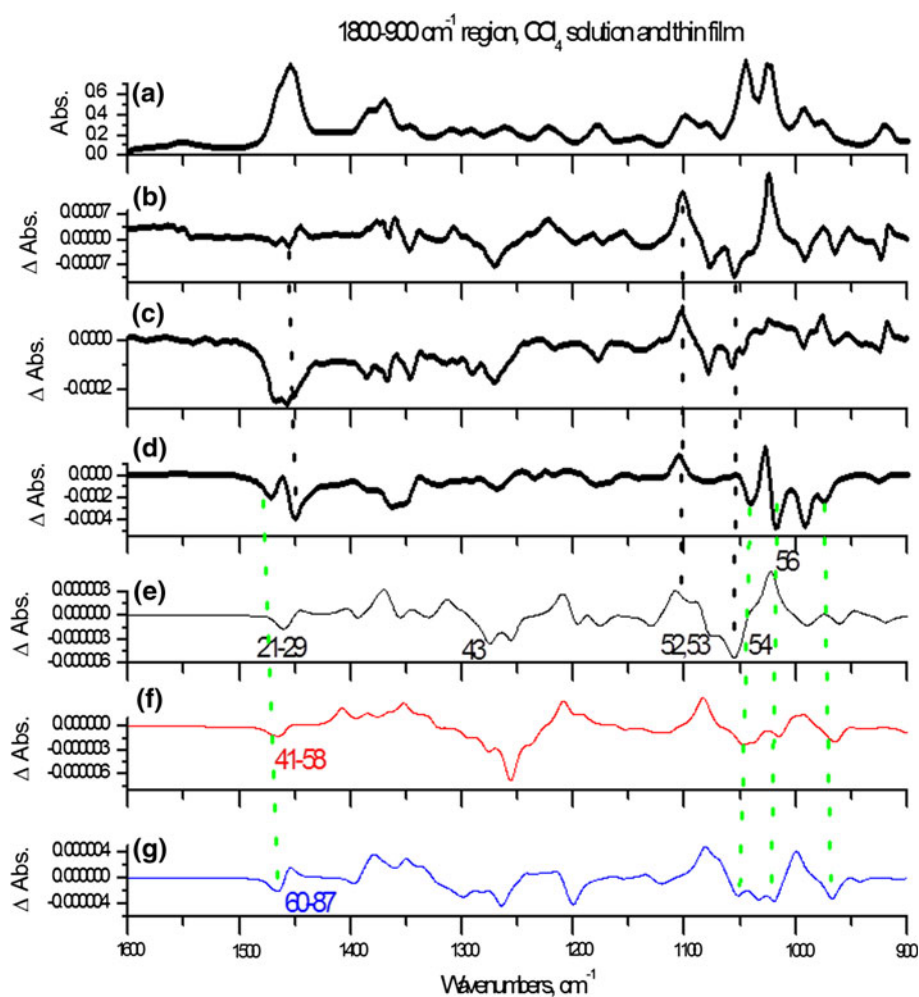
Nearly all the VCD signals in a and b can be assigned to the five most stable rotamers of the monomer; yet, we find some significant differences between the VCD spectra in film (d) and in solution, possibly due to the presence of the dimer and the trimer (bands marked with dotted lines). For example, in solution a negative band is seen at $1,455\text{ cm}^{-1}$. This band is clearly split in the film spectrum, where two negative VCD bands appear at $1,471$ and $1,448\text{ cm}^{-1}$. Other VCD features are observed in the film spectrum at $1,039$, $1,018$ and 991 cm^{-1} . In short, the solution spectra (b and c) are more precisely reproduced when the monomer spectra are accounted for. In the case of the film spectrum, the monomer, dimer and trimer must be taken into account.

Once again, the VCD technique provides insights where IR and Raman were unable to do so. IR and Raman spectra do not substantially change in this region, depending on experimental conditions.

The low-frequency region (below 400 cm^{-1} , Fig. 3) also presents a complex description in terms of PEDM analysis (Table 5S), where waggings, rockings and torsions of the constituent groups, and of the ring and ring deformations, all appear mixed to some extent.

Finally, we encounter substantial difficulties in comprehending the H-bonded structure as presented in the solid and in the concentrated CCl_4 solutions. In our opinion, structures other than the monomer, dimer and trimer exist. Although we were able to reproduce a representative part of the O–H region (along with the CH and $2,000\text{--}900\text{ cm}^{-1}$ regions), it was impossible to represent the whole range. This fact points to the presence of more complex H-bonded structures within the thin film spectra and concentrated solutions.

Fig. 5 Experimental and theoretical VCD spectra of (1R,2S,5R)-(–)-menthol in the 1,600–900 cm^{-1} spectral region: Recorded IR (a) and VCD (b) spectra (0.4 M in CCl_4 , 5,000 scans, 4 cm^{-1} of resolution, spacer of 0.15 mm); c recorded VCD spectrum (1.20 M in CCl_4 , 5,000 scans, 4 cm^{-1} of resolution, spacer of 0.05 mm); d recorded VCD spectrum (film, 5,000 scans, 4 cm^{-1} of resolution); e averaged sum of the predicted scaled spectra of the five most stable rotamers of the monomer (SQMFF methodology, in black); predicted scaled spectra of the dimer (f, in red) and trimer (g, in blue) (unique wavenumber scaling factor of 0.964 [43]). Parameters: pitch = 1 cm^{-1} , FWHM = 8 cm^{-1} (Color figure online)



Our strategy, as stated, was to tentatively study what kind of structures (other than monomers) could enhance comprehension of experimental data. Accordingly, Fig. 4c1 depicts the experimental VCD spectrum of a 0.30 M CCl_4 solution where the main features at 3,600–3,700 cm^{-1} can be attributed to the presence of the monomer, but the contribution of the oligomers is also evident. Meanwhile, Fig. 4b1 shows the experimental VCD spectrum of a 1.8 M CCl_4 solution where the main features can be assigned to oligomers (dimers, trimers and others), and no signature is found for the monomer. Finally, Fig. 5d shows the VCD spectrum for the thin film in the 2,000–900 cm^{-1} region. In this spectrum, the calculated VCD contributions of the monomers, the dimer and the trimer do not present very different features. Some characteristic features assigned to the monomers and oligomer would seem to constitute a reasonable approach (see 1,450 and 1,000 cm^{-1} regions) for confirming the presence of structures not pertaining to the monomer.

Conclusions

A systematic and detailed structural and vibrational study of the most stable conformers and rotamers of (1R,2S,5R)-(–)-menthol has been described. By taking into account the five most stable equatorial rotamers of the monomer, one dimer and one trimer of (–)-menthol, an analysis of the IR, Raman and VCD spectra of the title species can be accomplished both in solid (thin film) and in solution phases.

From the features of the recorded vibrational spectra, it is clear that the O–H group of (1R,2S,5R)-(–)-menthol takes part in a hydrogen bonding network. To reproduce experimental spectra, some dimers and trimers of menthol were optimized and their spectral features calculated. In the higher concentration solutions, bands of dimers and trimers were observed, whereas at lower concentrations features corresponding to the monomers were manifest.

It was found that VCD together with theoretical calculations provide enhanced information about the H-bonding

network for 4,000–900 cm^{-1} . In contrast, IR and Raman techniques are useful for this task only in the 4,000–3,200 cm^{-1} region.

Our study reveals the presence of at least five monomers, a dimer and a cyclic trimer when the IR–Raman–VCD spectra are obtained under different experimental conditions.

Acknowledgments This work was supported by the Junta de Andalucía (project P08-FQM-04096). The authors thank the University of Jaén for continuing financial support and its CICT for instrumental facilities. Juan Ramón Avilés Moreno expresses thanks to the Junta de Andalucía for a Post-Doc grant. We are grateful to a native English Speaker (Jean Louise Sanders) for reviewing the grammar. The authors are also grateful to D. Francisco Hermoso Torres for his help in the laboratory.

References

1. Wagner KH, Elmadfa I (2003) *Ann Nutr Metab* 47:95
2. Dembitsky VM (2006) *Lipids* 41:1
3. Eccles R (1994) *J Pharm Pharmacol* 46:618
4. Galeottia N, Mannellia LDC, Mazzantib G, Bartolinia A, Ghe-lardini C (2002) *Neurosci Lett* 322:145
5. Braina KR, Greena DM, Dykesb PJ, Marks R, Bola TS (2006) *Skin Pharmacol Physiol* 19:17
6. Caira MR, Griffith VJ, Nassimbeni LR, Van Oudtshoorn B (1996) *Supramol Chem* 7:119
7. Trujillo M, Morales EQ, Vazquez JT (1994) *J Org Chem* 59:6637
8. Parimoo P, Bharathi A, Mamatha D (1996) *Asian J Chem* 8:247
9. Albrecht M, Will J, Suhm MA (2010) *Angew Chem Int Ed* 49:6203
10. Nafie LA, Dukor RK, Roy JR, Rilling A, Cao X, Buijs H (2003) *Appl Spectrosc* 57:1245
11. Cao X, Shah RD, Dukor RK, Guo C, Freedman TB, Nafie LA (2004) *Appl Spectrosc* 58:1057
12. Laux L, Pultz V, Abbate S, Havel HA, Overend J, Moscovitz A (1982) *J Am Chem Soc* 104:4276
13. Abbate S, Longhi G, Ricard L, Bertucci C, Rosini C, Salvador P, Moscovitz A (1989) *J Am Chem Soc* 111:836
14. Castiglioni E, Lebon F, Longhi G, Abbate S (2002) *Enantiomer* 7:161
15. McCann JL, Rauk A, Wieser H (1998) *Can J Chem* 76:274
16. Mccann JL, Rauk A, Wieser H (1997) *J Mol Struct* 408(409):417
17. Barron LD, Hecht L, Blyth SM (1989) *Spectrochimica Acta A* 45:375
18. Coleman WM, Gordon BM, Lawrence BM (1989) *Appl Spectrosc* 43:298
19. Galisteo D, González-Vadillo ME, López Sastre JA, Martínez García MH, Rodríguez Amo JF (1994) *J Mol Struct* 326:239
20. Lassègues JC, Lascombe J (1982) *Vibrational spectra of gaseous hydrogen-bonded compounds*. In: Durig JE (ed) *Vibrational spectra and structure*, Chap. 2. Elsevier, Amsterdam
21. Zeegers-Huyskens T (1991) *Experimental vibrational characteristics of the hydrogen bond*. In: Huyskens PL, Luck WAP (eds) *Intramolecular forces. An introduction to modern methods and results*, Chap. 2. Springer, Berlin
22. Tuma C, Boese AD, Handy NC (1999) *Phys Chem Chem Phys* 1:3939
23. Del Bene JE, Jordan MJT (1999) *Int Rev Phys Chem* 18:119
24. Jeffrey GA (1997) *An introduction to hydrogen bonding*. Oxford University Press Inc., Oxford
25. Ignatyev IS, Partal F, López González JJ (2002) *J Phys Chem A* 106:11644
26. Xiaojing W, Yuanyuan C, Toshio Y (2007) *J Mol Spectrosc* 246:187
27. Shanmugam G, Polavarapu PL (2005) *Appl Spectrosc* 59:673
28. Deplazes E, van Bronswijk W, Zhu F, Barron LD, Ma S, Nafie LA, Jalkanen KJ (2008) *Theor Chem Acc* 119:155
29. Frisch MJ et al (2004) GAUSSIAN03, Revision E.01. Gaussian, Inc., Wallingford
30. Cheeseman JR, Frisch MJ, Devlin FJ, Stephens PJ (1996) *Chem Phys Lett* 252:211
31. Tomasi J, Mennucci B, Cammi R (2005) *Chem Rev* 105:2999
32. Fogarasi G, Pulay P (1985) *Vibrational spectra and structure*. In: Durig JE (ed) *Ab initio calculation of force fields and vibrational spectra*, Chap. 3. Elsevier, Amsterdam
33. Sundius T (1990) *J Mol Struct* 218:321
34. Sundius T (2002) *Vib Spectrosc* 29:89
35. Jasco Spectra Manager for Windows™
36. Larsen RW, Suhm MA (2010) *Phys Chem Chem Phys* 12:8152
37. Partal Ureña F, Avilés Moreno JR, López González JJ (2008) *Phys Chem A* 112:7887
38. Avilés Moreno JR, Partal Ureña F, López González JJ (2009) *Phys Chem Chem Phys* 11:2459
39. Partal Ureña F, Avilés Moreno JR, López González JJ (2009) *Tetrahedron Asymmetry* 20:89
40. Avilés Moreno JR, Partal Ureña F, López González JJ (2009) *Vib Spectrosc* 51:318
41. Avilés Moreno JR, Partal Ureña F, López González JJ (2011) *J Struct Chem* 1:67
42. Avilés Moreno JR, Ureña Homo E, Partal Ureña F, López González JJ (2011) *Spectrochimica Acta A* 79:767
43. NIST Standard Reference Database 101; Computational Chemistry Comparison and Benchmark DataBase: <http://cccbdb.nist.gov/vibscalejust.asp>